J. Fluid Mech. (1988), *vol.* 187, *pp.* 155–177
Printed in Great Britain

On the receptivity of free shear layers to two-dimensional external excitation

By THOMAS F. BALSA

Department of Aerospace and Mechanical Engineering, University of Arizona, Tucson, AZ 85721, USA

(Received 30 October 1986)

In this paper, we study the receptivity of a typical free shear layer to pulse-type and periodic excitation. We do this by solving the initial-value problem completely and studying its long-time behaviour. This leads to a wave packet for the pulse. By the superposition of many wave packets, we generate a spatial instability mode when the flow is convectively unstable. This establishes a general and simple relationship between the receptivities for pulse-type and sinusoidal excitations. We find that a shear layer is very receptive to high-frequency disturbances that are generated near the centreline of the layer.

1. Introduction

In the classical study of the stability of parallel shear flows, the concept of normal modes is an indispensable tool. Historically, most flows have been studied under the assumption of temporal stability (e.g. Betchov & Criminale 1967; Drazin & Reid 1981), although in the last twenty years it has become increasingly clear that the so-called spatial instability modes are more closely related to the disturbances, observed in experiments on sinusoidally excited flows, than are the temporal ones (for early and recent accounts, see Michalke 1965 and Gaster, Kit & Wygnanski 1985). If a mode is assumed to be proportional to $[\exp(\omega t)\exp(+ikx)]$, then in the temporal and spatial theories we respectively have: $k_I = 0$, ω complex; $\omega_R = 0$, k complex; where the subscripts R and I denote the real and imaginary parts of a complex number and $\omega = \omega(k)$ is the complex dispersion relation.

While studies of normal modes can usually shed light on the stability of the flow, such studies say nothing about when and how the modes actually evolve and how their amplitudes are related to the strength of the input disturbance. The relationship between the mode amplitude and the external disturbance is called the *receptivity* of the flow. Our main objective is to study the receptivity of mixing layers. Quite unlike the work of Goldstein (1983), in which he examines the generation of instability waves by free-stream disturbances incident on a flat-plate boundary layer, the present paper deals with the generation of instability waves by the 'creation' (say, by a small oscillating flap) and convection of concentrated vorticity within a mixing layer.

The study of receptivity is intimately connected with the initial-value problem and the excitation of the various instability modes by the initial disturbance. A pioneering study along these lines was made by Criminale & Kovasznay (1962). They examined the evolution of localized disturbances in a laminar boundary layer and described the physical characteristics of the wave packets into which these disturbances eventually develop. They also advanced the very useful and powerful

idea of approximating the growth rate/wavenumber relationship by the osculating quadratic surface centred about the most unstable vector wavenumber. This approximation may be used to develop a unified and highly geometric theory for wave packets in arbitrary parallel shear flows.

In his classic work on wave packets in boundary layers, Gaster (1968, 1975) continued the departure from a purely modal analysis. He considered the simultaneous evolution of many unstable modes and found that these interfered with each other, so that the principal contribution of all these modes at a given point in the flow and at a given instant of time came from a single wavenumber, $k = k(x, t)$, which is, in fact, complex. Because of this, Gaster could deduce many of the important and interesting properties of the packet, without explicitly addressing the receptivity issue or solving the initial-value problem.

A very similar study was carried out by Huerre & Monkewitz (1985) (for a free shear layer) with a totally different objective. Their principal aim was to study the conditions under which spatial instability modes evolve in a harmonically excited flow. They do this by studying the branch-point singularities of the complex dispersion relation for a family of *tanh* base velocity profiles. Roughly speaking, they find that spatial instability modes cannot evolve when there is a significant amount of reverse flow. In this case, the instability is termed *absolute*. On the other hand, when the external streams are coflowing, the instability is *convective*, and the large-(x, t) behaviour of the solution is identical with that of the spatial instability mode at the excitation frequency ω_*.

The present work, though closely related to these very important previous papers, takes the analysis and physics one step further, by establishing and studying the explicit functional relationships between the input disturbances and the amplitudes of the wave packet, and of the spatial instability mode, they generate. Our basic building block is a packet, and we begin with its rigorous derivation and a review of its characteristics in a particularly simple base flow.

Next, we discuss one of the new ideas of this paper. This deals with the representation of a spatial instability mode in terms of wave packets. It is shown how the superposition of a certain set of packets leads to a mode – this result is important for two reasons. First, it establishes a very simple and general connection between the amplitude of the packet and that of the mode; the former is simply the (complex) group velocity multiplied by the latter. Secondly, this superposition idea proves almost indispensable in the study of three-dimensional spatial instability modes generated by sinusoidally oscillating and spatially compact sources.

Finally, we study the receptivity of a free shear layer to pulse-type and harmonically oscillating disturbances. The base velocity profile that we use is shown in figure 1: it consists of three straight-line segments joined by smooth curves, confined to the immediate edges of the layer. The entire velocity profile is infinitely differentiable. The high-Reynolds-number viscous instability of this flow (both temporal and spatial) is almost identical with the inviscid instability of the corresponding piecewise linear profile (Balsa 1987). Therefore, closed-form expressions can be found for all quantities of interest (e.g. dispersion relations), and all mathematical manipulations (e.g. contour deformations) can be justified rigorously. This flow serves as a good model for more general free shear layers as confirmed by our comparison of wave packets in this flow and in a tanh profile.

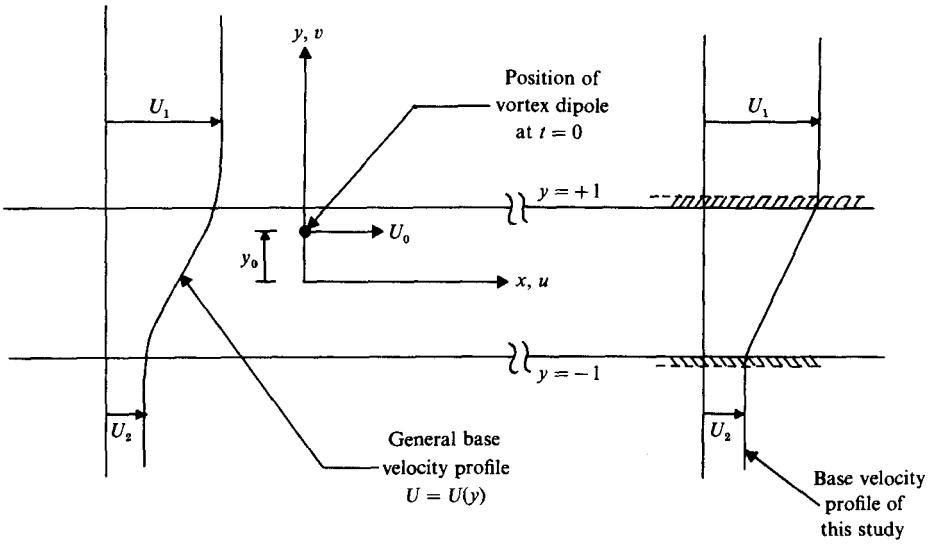

FIGURE 1. Geometry of the problem.

2. Formulation of the problem

Let (x, y) be a Cartesian coordinate system and denote time by t. Consider a unidirectional, incompressible, and inviscid parallel shear flow at constant pressure whose velocity components are $[U(y), 0]$ and suppose this flow is perturbed by a small disturbance whose precise form will be specified momentarily (figure 1). The disturbance stream function $\Psi = \Psi(x, y, t)$ and the perturbation vorticity $\zeta = \zeta(x, y, t)$ are assumed to satisfy the inviscid linearized equations of motion

$$\nabla^2 \Psi = -\zeta, \tag{1a}$$

$$\frac{\partial \zeta}{\partial t} + U\frac{\partial \zeta}{\partial x} - v\frac{\mathrm{d}^2 U}{\mathrm{d}y^2} = -\delta'(x)\,\delta(y-y_0)\,\delta(t), \tag{1b}$$

where $\nabla^2 = \partial^2/\partial x^2 + \partial^2/\partial y^2$ is the two-dimensional Laplacian and $(u, v) = (\partial\Psi/\partial y, -\partial\Psi/\partial x)$ are the perturbation velocity components in the x- and y-directions, respectively.

The perturbations in the flow are produced by a two-dimensional compact vortex dipole which is deposited into the flow at the point $x = 0$ and $y = y_0$. This vortex dipole is represented by the right-hand side of (1*b*). The transverse source coordinate y_0 is arbitrary, and there is no loss in generality by taking the x-coordinate of the dipole to be zero. The vortex dipole is deposited instantaneously at $t = 0$ but, of course, once it is placed in the flow, it will persist and be convected by the flow. Implicit in the previous remarks is the observation that $\delta(\xi)$ denotes the usual delta function, with support at $\xi = 0$, and $\delta'(\xi) = \mathrm{d}\delta(\xi)/\mathrm{d}\xi$.

We shall refer to $\Psi = \Psi(x, y, t)$ as the Green function, although it would be more customary to do so for the case in which $\delta'(x)$ in (1*b*) is replaced by $\delta(x)$. We use $\delta'(x)$ for two reasons. First, mathematically speaking, we wish to ensure that the Fourier transform (in x) of Ψ exists in the classical (i.e. non-distributional) sense for all values of time. This clearly facilitates the contour deformations at infinity. Had we used $\delta(x)$ in place of $\delta'(x)$, the stream function at $t = 0^+$ would have been

$\Psi \sim \log[x^2+(y-y_0)^2]^{\frac{1}{2}}$; this function does not have a classical Fourier transform. Secondly, physically speaking, a single dipole provides a crude representation of the flow field produced by a trailing-edge flap (Gaster *et al.* 1985) which is moved quickly (i.e. impulsively) up and then stopped. Owing to the sharp edge of the flap, this motion generates starting and stopping vortices of opposite signs – these we interpret as the two elementary vortices comprising the dipole. It seems quite reasonable to assume that oscillating ribbons and flaps generate a continuous train of dipoles and the excitation of the instability waves in a mixing layer occurs through the deposition of these dipoles in the flow. Finally, once Ψ is known, the solution of our governing equations, with an arbitrary right-hand side in (1*b*), can be written down immediately by formal convolution integrals. In fact, in §5, we use the forcing function $[-\delta'(x)\delta(y-y_0)\cos(\omega_* t)]$ to represent a harmonically oscillating dipole (ω_* = radian frequency of oscillation), and the solution for the source problem is the present solution divided by $(-ik)$, where k is a suitable (complex) wavenumber.

The initial and boundary conditions are as follows:

$$\Psi = \zeta = 0 \quad \text{for } t < 0^-, \tag{2a}$$

$$u, v, \zeta \to 0 \quad \text{for } (x^2+y^2)^{\frac{1}{2}} \to \infty. \tag{2b}$$

In other words, we are looking for the causal response of the flow generated by the dipole. It will prove to be convenient to transfer the initial conditions to $t = 0^+$ by integrating (1*b*) across $t = 0$ to obtain the vorticity and then solving (1*a*). The final results are

$$\zeta(x, y, 0^+) = -\delta'(x)\,\delta(y-y_0), \tag{3a}$$

$$\Psi(x, y, 0^+) = \frac{1}{2\pi}\frac{x}{x^2+(y-y_0)^2}, \tag{3b}$$

which clearly coincide with the classical flow generated by our vortex dipole in the absence of a mean shear. For $t > 0$, the right-hand side of (1*b*) vanishes, so we may think of (1), (2*b*) as a homogeneous problem (for $t > 0^+$) with initial conditions (3).

Before we write down the Green function, there are several issues that need discussion. First, the perturbations are assumed to be incompressible and inviscid. The assumption of incompressibility carries with it the usual restrictions to low-Mach-number flows. On the other hand, the assumption of zero viscosity is more difficult to justify with any kind of generality. It is clear from figure 1 that the general base velocity profile under consideration, $U = U(y)$, will have (exactly) one inflexion point and is likely to be unstable to inviscid perturbations. This implies that, in certain regions of complex wavenumber space, the inviscid and high-Reynolds-number instabilities of the base flow are virtually identical. (For example, this is certainly the case for $U \sim \tanh y$.) On the other hand, there also exist regions in wavenumber space in which the solutions to the Rayleigh and Orr–Sommerfeld equations are quite different (even in the case of very large Reynolds number); in fact, in these latter regions the inviscid results are physically meaningless.

Unfortunately, these various regions in complex wavenumber space have not been identified as yet, even for the tanh profile. The situation is not much different for other flows, such as wakes or jets (Mattingly & Criminale 1972; Betchov & Criminale 1966). Because of this it is very difficult to generally justify the validity of the contour deformations used in the inversion of the Fourier integrals (see §4) on the basis of purely inviscid theory. On the other hand, the spectrum of the Orr–Sommerfeld operator (for the tanh profile) is not known (the work of Tatsumi,

Gotoh & Ayukawa 1964 is very limited in this context) so that we are forced to examine a model problem whose instability characteristics (viscous as well as inviscid) are rather incompletely understood.

For these reasons, in this paper, we shall study the characteristics of the Green function in a base flow, which is also shown in figure 1. Essentially, $U = U(y)$ is linear between the two edges of the shear layer (at $y = \pm 1$), and this straight-line segment is joined to the external streams in two very narrow regions at the shear-layer edges. The entire profile is assumed to be infinitely smooth. The viscous instabilites of such a profile were studied elsewhere (Balsa 1987). It was found that, at large Reynolds numbers, these are virtually identical with the inviscid instabilities of a piecewise linear profile of Rayleigh at all finite (complex) wavenumbers. This profile is given by

$$U(y) = \begin{cases} U_1 = \text{const} & (y > 1), \\ U_m + \frac{1}{2}\Delta U\, y & (|y| \leqslant 1), \\ U_2 = \text{const} & (y < -1), \end{cases} \tag{4}$$

where $U_m = \frac{1}{2}(U_1 + U_2)$ and $\Delta U = U_1 - U_2$.

The point is that the inviscid Green function of our piecewise linear profile (4) is only very slightly different from its viscous counterpart for a class of base velocity profiles described in the previous paragraph (see also figure 1). Since the initial-value problem (1), (2), with $U(y)$ given by (4), can be solved in closed form, we have the distinct advantage of providing functional relationships among variables. Because of this, the piecewise linear shear layer serves as a useful model for more general free shear flows, especially in the context of complex three-dimensional disturbances or unsteady effects (Greenspan & Benney 1963). In fact, the quantitative differences between wave packets in the tanh and piecewise linear shear layers are quite small.

The evolution of certain wavelike disturbances in unbounded shear flows, with spatially uniform shear rates, has been studied by Craik & Criminale (1986) in a very general setting. These so-called Kelvin waves may also be described, in terms of a modal decomposition, as arising from the continuous spectrum of the Orr–Sommerfeld operator. It is possible to write our solution (see (9)) as a superposition of Kelvin (i.e. continuous) and Rayleigh (i.e. discrete) modes, and indeed this approach of superposition has been explicitly used by Farrell (1982, 1984) in the study of atmospheric problems.

Farrell (1984) finds that for certain initial conditions, the disturbances in a baroclinic instability may initially grow to large enough amplitudes, owing to the continuous modes, that nonlinear effects become important before the (exponential) normal modes develop to any significant degree. We do not believe that this scenario usually occurs in free shear flows, in view of the success of Gaster *et al.* (1985) in describing the large-scale structures using Rayleigh modes. The coupling between continuous and discrete modes occurs at boundaries and interfaces (Farrell 1984).

Perhaps it is also wise to say a few words about the two-dimensionality of our assumed flow. Certainly, the evolution of three-dimensional wave packets and instability waves is a very relevant and important subject and, in principle, our two-dimensional results may be obtained from the corresponding three-dimensional ones by the 'method of descent of dimension'. This procedure is usually quite cumbersome and, almost always, two- and three-dimensional results are obtained from separate analyses. Our considerable interest in detailed two-dimensional results is motivated by a parallel experimental effort (Glezer, Wygnanski & Balsa 1986).

3. The Green function

Our governing equations (1a, b) are solved by Fourier transforms in the x-direction. Introduce transform pairs by

$$(\hat{\cdot}) = \frac{1}{(2\pi)^{\frac{1}{2}}} \int_{-\infty}^{\infty} (\cdot)\, \mathrm{e}^{-\mathrm{i}kx}\, \mathrm{d}x, \tag{5a}$$

$$(\cdot) = \frac{1}{(2\pi)^{\frac{1}{2}}} \int_{C} (\hat{\cdot})\, \mathrm{e}^{+\mathrm{i}kx}\, \mathrm{d}k, \tag{5b}$$

where k is the streamwise or axial wavenumber. In general, k is complex and C is a suitably chosen contour. The transforms of (1a, b) are, for $t \geqslant 0^+$,

$$\left(\frac{\partial^2}{\partial y^2} - k^2\right)\hat{\Psi} = -\hat{\zeta}, \quad \left(\frac{\partial}{\partial t} + \mathrm{i}kU\right)\hat{\zeta} = 0, \tag{6a, b}$$

where, for our piecewise linear profile, $U'' = 0$. Equations (6a, b) are partial differential equations in (y, t) for $\hat{\Psi}$ and $\hat{\zeta}$ at parameter values of the wavenumber k. The initial conditions at $t = 0^+$ are

$$\hat{\zeta} = -\frac{\mathrm{i}k}{(2\pi)^{\frac{1}{2}}}\delta(y - y_0), \tag{7a}$$

$$\hat{\Psi} = -\frac{\mathrm{i}k}{2(2\pi)^{\frac{1}{2}}\kappa} \exp\left[-\kappa|y - y_0|\right]. \tag{7b}$$

Note that

$$\kappa = (k^2)^{\frac{1}{2}} = \begin{cases} +k & \text{for } k_{\mathrm{R}} > 0, \\ -k & \text{for } k_{\mathrm{R}} < 0, \end{cases} \tag{8}$$

where $k_{\mathrm{R}} = \mathrm{Re}\,(k)$. This implies that the origin is a double branch point with the two branch cuts extending along the positive and negative imaginary axes. Therefore, the solution will have certain symmetries about the $k_{\mathrm{R}} = 0$ line, and it is sufficient to confine our attention to the half-space $k_{\mathrm{R}} > 0$.

For our piecewise linear profile, the vorticity equation (6b) can be integrated once and for all. The solution for the stream function $\hat{\Psi}$ is readily expressible as linear combinations of $\exp(\pm\kappa y)$. The algebra is quite involved and, for this reason, some of the details and intermediate results are relegated to the Appendix. Here, we remind the reader that across the interfaces, whose mean locations are at $y = \pm 1$, the Fourier transforms of the transverse velocity component $\hat{v}$ and the pressure are continuous. Finally, we must consider three separate classes of problems depending on the transverse location of the vortex dipole, according to the inequalities $y_0 > 1$, $|y_0| \leqslant 1$, and $y_0 < -1$. By far the most important case is the second one, in which the shear layer is excited by a source that is within the layer. We now give the solution for this case; the solutions for the other cases may be found in the Appendix.

Perhaps it is worthwhile to point out that these solutions are obtained without the use of a Laplace transform in time; in the problem under consideration, a Laplace transform is not necessary.

In order to keep the equations and results manageable, we focus on the transverse

velocity component v at the upper interface $y = +1$. Similar results hold for the other physical quantities of interest. From the Appendix, we have

$$(2\pi)^{\frac{1}{2}}v(x,1,t) = \int_{-\infty}^{\infty} \mathrm{e}^{\mathrm{i}kx}\{\mathscr{F}_1(k)\exp[\omega_1(k)t] + \mathscr{F}_2(k)\exp[\omega_2(k)t] + a(k)\exp(-\mathrm{i}kU_0 t)\}\,\mathrm{d}k. \quad (9)$$

Note that the Fourier inversion contour is nominally chosen along the real axis (although this contour will be deformed momentarily) and (9) is valid for all positive values of time. Equation (9) is an exact solution to (1), (2). Very roughly speaking, the initial disturbance in the flow is resolved into two Rayleigh modes with dispersion relations $\omega_j(k)\,(j = 1,2)$ and a 'convected mode' represented by the last term in (9).

The various expressions in (9) are as follows:

$$\left.\begin{matrix}\omega_1(k)\\ \omega_2(k)\end{matrix}\right\} = -\mathrm{i}kU_{\mathrm{m}} \pm \frac{\Delta U\lambda(k)k}{\kappa}, \quad (10a)$$

$$\left.\begin{matrix}\mathscr{F}_1(k)\\ \mathscr{F}_2(k)\end{matrix}\right\} = \frac{(A_0-a)(\lambda \pm \mathrm{i}a_{11}) \pm \mathrm{i}a_{12}(B_0-b)}{2\lambda}, \quad (10b)$$

where

$$\lambda = \lambda(k) = \tfrac{1}{4}[\mathrm{e}^{-4\kappa} - (1-2\kappa)^2]^{\frac{1}{2}}, \quad (10c)$$

$$\left.\begin{matrix}A_0 = A_0(k)\\ B_0 = B_0(k)\end{matrix}\right\} = -\frac{\kappa}{2(2\pi)^{\frac{1}{2}}}\mathrm{e}^{-\kappa}\,\mathrm{e}^{\pm\kappa y_0}, \quad (10d)$$

$$\left.\begin{matrix}a = a(k)\\ b = b(k)\end{matrix}\right\} = \frac{k^2}{4(2\pi)^{\frac{1}{2}}}(y_0 \mp 1) \times \frac{\sinh[\kappa(y_0 \pm 1)][\tfrac{1}{2}\mathrm{e}^{-2\kappa} \mp (y_0 \pm 1)\Gamma(k)] \pm (y_0 \pm 1)\Gamma(k)\,\mathrm{e}^{-2\kappa}\sinh[\kappa(y_0 \mp 1)]}{\mathscr{D}(k)}, \quad (10e)$$

$$a_{11} = a_{11}(k) = \tfrac{1}{4} - \Gamma(k)\cosh 2\kappa, \quad (10f)$$

$$a_{12} = a_{12}(k) = \Gamma(k) - \tfrac{1}{4}\mathrm{e}^{-2\kappa}, \quad (10g)$$

$$\Gamma = \Gamma(k) = \frac{\kappa}{2\sinh 2\kappa}, \quad (10h)$$

$$\mathscr{D}(k) = (\tfrac{1}{2}\kappa y_0)^2 + \lambda^2(k). \quad (10i)$$

Recall that y_0 is the transverse coordinate of the dipole, $U_0 = U(y_0)$, $U_{\mathrm{m}} = \frac{1}{2}(U_1 + U_2)$, and $\Delta U = U_1 - U_2$.

In (10c), we choose the principal square root such that $Z^{\frac{1}{2}}$ maps the complex Z-plane cut along the negative real axis onto the half-space $\mathrm{Re}\,(Z^{\frac{1}{2}}) > 0$. This can be accomplished very simply on the computer by calling the FORTRAN intrinsic function CSQRT. Furthermore, without any loss of generality, we can assume that $\Delta U > 0$ so that ω_1 unambiguously represents the unstable dispersion relation for $k_{\mathrm{R}} > 0$. The branch-point singularity of ω_1 is discussed in the next section.

4. The long-time behaviour of the Green function–wave packet

Our principal objective in this section is the derivation of the long-time behaviour of $v(x, 1, t)$. This yields a wave packet whose spatial and temporal characteristics are obtained by applying the saddle-point method to (9). The method, pioneered in this context by Gaster (1968), is now well known. Although we shall show a couple of interesting results for wave packets, our main interest in them stems from the fact that spatial instability modes can be interpreted very nicely in terms of these packets. This idea is discussed fully in the next section. In addition, we shall rigorously show the kind of contour deformations that are permissible in the Fourier inversion – this can be done because our solution is known in closed form. Note that, in general, it is not possible to close the integration contours at infinity.

Since the wave packet is convected by the flow, it is simplest to observe it in a moving coordinate system. Let

$$x = Gt, \tag{11a}$$

where G is the observer speed. (It turns out that G is also the (real) group velocity.) A related, but somewhat more useful, quantity is

$$\mathscr{G} = \frac{G - U_2}{\Delta U} = \frac{x/t - U_2}{\Delta U}, \tag{11b}$$

so that expression (9) for $v(x, 1, t)$ may be rewritten as

$$(2\pi)^{\frac{1}{2}} v(x, 1, t) = \sum_{j=1}^{3} \int_0^\infty \mathscr{F}_j(k) \exp[h_j \tau] \, \mathrm{d}k + \text{c.c.}, \tag{12a}$$

where $\tau = \Delta U t > 0$, $\mathscr{F}_3(k) = a(k)$, c.c. denotes the complex conjugate of all the terms preceding it on the right-hand side of an equation, and

$$h_j = h_j(k, \mathscr{G}) = \mathrm{i}k(\mathscr{G} - \tfrac{1}{2}) \pm \lambda(k) \quad \text{for } j = 1, 2, \tag{12b}$$

$$h_3 = h_3(k, \mathscr{G}) = \mathrm{i}k\left[\mathscr{G} + \frac{U_2 - U_0}{\Delta U}\right]. \tag{12c}$$

Note that $\mathscr{F}_j (j = 1, 2, 3)$ do not depend on the external streams U_1 and U_2. Insofar as the long-time behaviour of the solution is dominated by the unstable mode (i.e. $\mathscr{F}_1$ and h_1), all (inviscid) wave packets in a given base flow are dynamically similar provided that the scaled variable $\tau = \Delta U t$ is used to measure time and the streamwise behaviour is expressed as a function of $\mathscr{G}$.

We now wish to evaluate (12a) for large values of time but at fixed values of G or $\mathscr{G}$. The integrand of (12a) turns out to be an analytic function of k for $k_R > 0$, although this result is by no means obvious from a casual inspection. Very briefly, $\lambda(k)$ has a branch-point singularity at $k = k_N \approx 0.6392$ and no other singularity in the finite part of (complex) wavenumber space. On the other hand, $\mathscr{D}(k)$ has a double zero at the origin and a simple zero on the real axis. This latter zero lies in the region $k_R \geqslant k_N$ and depends on the location of the dipole y_0. In spite of these zeroes of $\lambda(k)$ and $\mathscr{D}(k)$, the total integrand of (12a) has no poles or branch-point singularities! The last remark should be quite obvious from the problem formulation, as expressed by (6) and (7). Because of these observations, the path of integration may be chosen slightly above (or below) the real axis.

On the other hand, if the individual terms in the integrand are considered separately [e.g. $\mathscr{F}_1 \exp(h_1 \tau)$], which is really quite necessary for the efficient

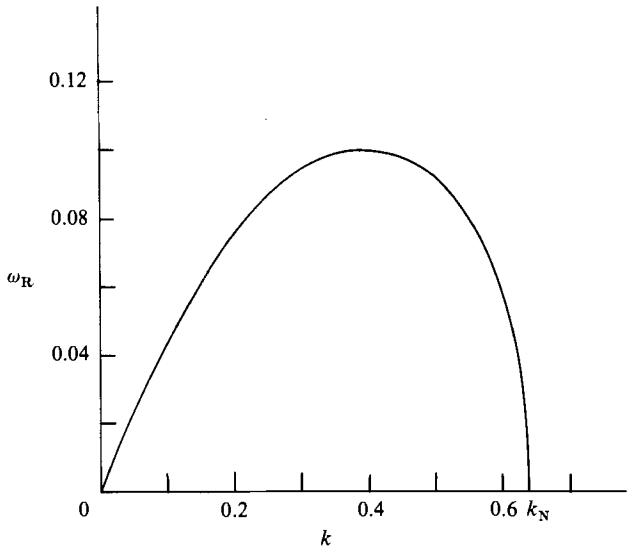

FIGURE 2. Growth rate of unstable mode in piecewise linear base flow as a function of wavenumber ($U_1 = 1$, $U_2 = 0$).

evaluation of (12a), the branch cut and poles arising from $\lambda(k)$ and $\mathscr{D}(k)$ must be taken into account.

It is worthwhile to digress at this point to discuss the temporal stability of our base velocity for the special profile $U_1 = 1$, $U_2 = 0$, and $\Delta U = 1$. In this case, $k_I = 0$ and $0 \leqslant k_R \leqslant k_N$, where k_N is the neutral wavenumber (obtained numerically). The phase velocity is $U_m = \frac{1}{2}(U_1 + U_2) = \frac{1}{2}$ and the growth rate ω_R is given in figure 2, where ω_R is the real part of the unstable eigenvalue ω_1. Comparing these results with those of Michalke (1964) for the tanh profile, we find very good semiquantitative agreement for the growth rates and perfect agreement for the phase velocity. It is only in the vicinity of the corresponding neutral points that the two growth rates differ. For the purposes of the present analysis, this difference is largely irrelevant since the dominant contribution to integral (12a) comes from a complex wavenumber that is far from the neutral point. The point $k = k_N$ is a branch point, and the branch cut (of ω_1, ω_2, or λ) extends from k_N to plus infinity along the real axis.

Because of the presence of $\lambda(k)$ (see (10b)) in $\mathscr{F}_1$ and $\mathscr{F}_2$, both of these latter functions have a square-root singularity at the neutral point $k = k_N$ and a branch cut along the real axis to the right of k_N. In addition, for $y_0 > 0$, $\mathscr{F}_2$ has a pole on the branch cut at $k = k_p > k_N$ arising from the zero of the determinant, $\mathscr{D}(k_p) = 0$. (For $y_0 < 0$, the same remark holds for $\mathscr{F}_1$; for $y_0 = 0$, $\mathscr{F}_1$ and $\mathscr{F}_2$ have simple poles at $k = k_N = k_p$.) Note that k_p is a monotonically increasing function of $|y_0|$ such that $k_p = k_N$ for $y_0 = 0$. Finally, $a(k) = \mathscr{F}_3$ has a simple pole at k_p; the singularities at $k = 0$ are removable.

We are now in a position to evaluate (12a) as $\tau = \Delta U t \to \infty$. We shall do this for the case $\mathscr{G} > 0.5$ (for $\mathscr{G} < 0.5$, we can reflect the contours obtained in the present case about the real axis). The nominal contour of integration is chosen very slightly above the real axis (figure 3).

The principal contribution of the third term ($j = 3$) of (12a) for large times comes either from the endpoint $k = 0$ or the pole $k = k_p$, depending on whether $[\mathscr{G} + (U_2 - U_0)/\Delta U]$ is positive or negative. In either case, this contribution is no larger than order unity.

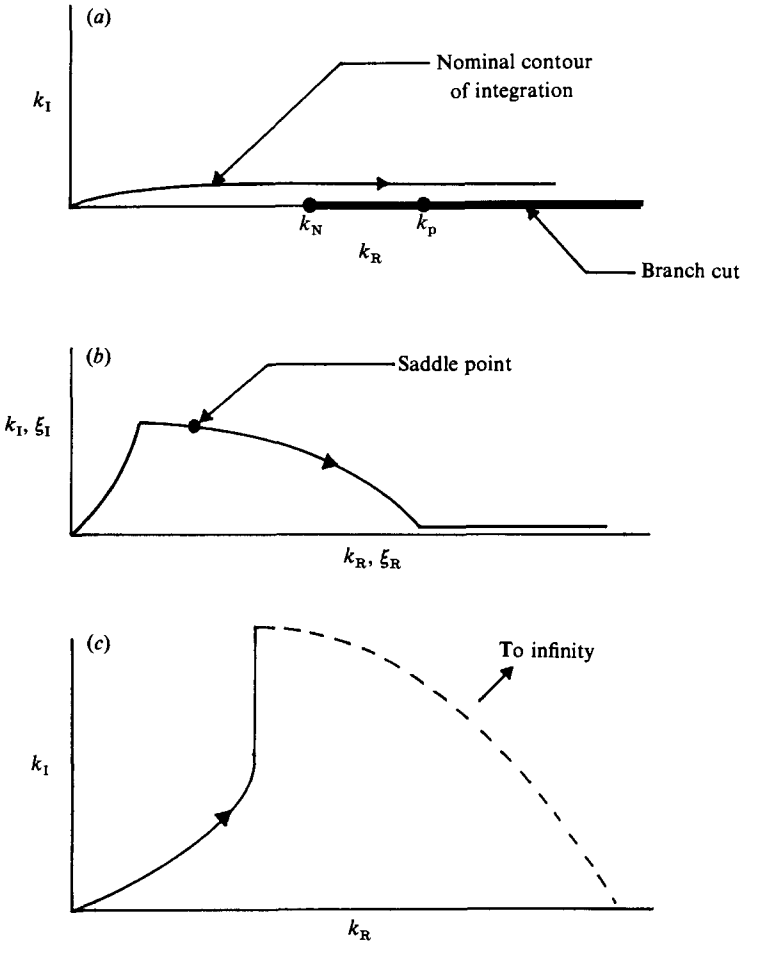

FIGURE 3. Deformed contours of integration for wave packet: (*a*) for original integral and $\mathscr{F}_3$, (*b*) for $\mathscr{F}_1$, and (*c*) for $\mathscr{F}_2$.

For the second term ($j = 2$), we deform the contour in the first quadrant into the curve $\mathrm{Im}\,(h_2) = 0$ which passes through the origin and extends to infinity. There is no difficulty in closing the contour at infinity with zero contribution to the integral. Along this deformed contour, $\mathrm{Re}\,(h_2)$ is non-positive and monotonically decreasing. Hence, the integral is of the Laplace type, whose dominant contribution comes from $k = 0$. This contribution is at most of the magnitude $O(1/t)$ as $t \to \infty$.

Finally, consider the first term ($j = 1$) of (12*a*). Here, we have a saddle point in the first quadrant. We deform the nominal contour of integration in the following manner. From the origin $k = 0$, we go along the level curve $\mathrm{Re}\,(h_1) = 0$ in the first quadrant until we intersect the curve of constant phase through the saddle point. This can always be done. We then jump onto this latter curve and pass through the saddle point so that $\mathrm{Im}\,(h_1) = \mathrm{const}$ and $\mathrm{Re}\,(h_1)$ reaches a local maximum (positive) at the saddle point. Finally, this saddle-point curve always intersects the top of the branch cut to the right of the neutral point, and we integrate out to infinity along the top of the branch cut. It is not possible to deform the contour at infinity. The dominant contribution to the integral comes from the saddle point since $\mathrm{Re}\,(h_1)$ is positive there. Contributions from the endpoints of the integral or (possibly) from the

pole at k_p are exponentially small relative to the saddle-point contribution. We now calculate this dominant contribution. The various contours are shown in figure 3.

For notational simplicity, we drop the subscript on h_1 so that $h(k, \mathscr{G}) = h_1(k, \mathscr{G})$. Then the saddle point $k_0 = k_0(\mathscr{G})$ satisfies

$$h_k(k_0, \mathscr{G}) = 0 \tag{13}$$

(Duff & Naylor 1966, p. 318), where $h_k = \partial h/\partial k$. Recall that the velocity $\mathscr{G}$ is real but $k_0 = k_0(\mathscr{G})$ is, in general, complex. Hence, for large values of time, (12*a*) becomes

$$v(x, 1, t) = \frac{1}{[-\tau h_0^+(\mathscr{G})]^{\frac{1}{2}}} \mathscr{F}_1(k_0) \exp[\tau h_0(\mathscr{G})] + \text{c.c.}, \tag{14a}$$

where

$$\tau = \Delta U t,$$

$$h_0(\mathscr{G}) = h(k_0, \mathscr{G}), \tag{14b}$$

$$h_0^+(\mathscr{G}) = h_{kk}(k_0, \mathscr{G}), \tag{14c}$$

and

$$h_{kk} = \frac{\partial^2 h}{\partial k^2}.$$

The reader will notice the extreme care that we have exercised in deforming the contour of integration and in studying the global singularities of the integrand in (12*a*). This is a pivotal step in order to ensure that the correct saddle point is chosen in the evaluation of the integral (Mattingly & Criminale 1972). Even in the relatively simple case of the piecewise linear profile, both of the functions $h_1(k, \mathscr{G})$ and $h_2(k, \mathscr{G})$ have many saddle points, but only one of these is admissible in the sense of Bleistein & Handelsman (1975, p. 267). Very crudely speaking, however, the dominant contribution to the Green function at each observer velocity $\mathscr{G}$ comes from 'the' saddle point of the 'most unstable mode'. We believe that this long-time solution may be obtained from an inviscid analysis since the flow is unstable. On the other hand, if the initial disturbance contained only stable wavenumbers, one could not have obtained the long-time solution without the inclusion of viscosity. Results along the lines leading to (14*a*) have been obtained by Criminale & Kovasznay (1962), Gaster (1968), and Huerre & Monkewitz (1985); one objective of this paper is to compare the characteristics of wave packets in the tanh and piecewise linear profiles. A second objective is to describe a (linear) spatial instability mode as a superposition of packets.

5. Spatial instability

The subject of spatially growing modes or simply spatial instability is not without controversy (Drazin & Reid 1981, p. 147), yet experimental data for periodically forced shear layers clearly indicate that, in the initial part of the layer, where the disturbances are still relatively weak, linear spatial stability theory provides better agreement with data than does temporal theory. (For early and recent accounts, see Michalke 1965 and Gaster *et al.* 1985.) The purpose of the present section is to show how a spatial mode arises from the initial-value problem via a suitable superposition of wave packets. This is diametrically opposite but, of course, complementary, to the work of Gaster (1975) in which a wave packet in a boundary layer is synthesized from a large set of instability modes.

Historically, the initial-value problem has been attacked by a combination of

Fourier–Laplace transforms. In the present paper, we have avoided the use of a Laplace transform in time for the sake of simplicity. In a similar spirit, the solution to the harmonically forced shear layer is expressed in terms of a Duhamel-type integral

$$\psi(x,y,t) = \int_0^t \Psi(x,y,T)\cos[\omega_*(t-T)]\,\mathrm{d}T, \tag{15a}$$

$$= \tfrac{1}{2}\mathrm{e}^{\mathrm{i}\omega_* t}\int_0^t \Psi(x,y,T)\,\mathrm{e}^{-\mathrm{i}\omega_* T}\,\mathrm{d}T + \text{c.c.}, \tag{15b}$$

where $\psi(x,y,t)$ is the stream function associated with the harmonic problem. In this case, the forcing term on the right-hand side of (1*b*) is replaced by $[-\delta'(x)\,\delta(y-y_0)\cos(\omega_* t)]$, where ω_* is the (real) frequency of the oscillations. Hence, vortex dipoles are introduced into the flow continuously at $x = 0$, $y = y_0$ in a way that is roughly reminiscent of the effects of an oscillating splitter-plate flap. Note that in (15), $\Psi(x,y,T)$ is the Green function.

We are interested in the solution of the harmonic problem for large but fixed values of the streamwise coordinate x, in the 'steady state' as $t\to\infty$. The meaning of (15*b*) becomes especially clear in terms of an (x,T)-wave diagram (figure 4). The pulse generating the fundamental solution is emitted at $x = T = 0$. In the shaded region surrounding the origin, the Green function evolves into its asymptotic structure. In the wedge bounded by $x/T = U_1, U_2$ this asymptotic structure is precisely the wave packet (14*a*). We have not calculated the asymptotic solution outside the wedge (although we could easily do so) because it is, in fact, exponentially small (in a relative sense).

Now the range of integration in (15*b*) is the interval $0 \leqslant T \leqslant t$ so that as $t\to\infty$ the observer point D, with coordinates (x,t), recedes to infinity. Therefore, the principal contribution to integral (15*b*) comes from the entire interval BC; this interval contains the exponentially large part of the wave packet. The contributions from intervals AB and CD are exponentially small (in a relative sense) and, therefore, negligible. Clearly, the previous remarks are valid as long as x is large enough (so that the line $x = \text{const}$ does not intersect the shaded region of figure 4) and U_1 and U_2 are positive. The case where $U_2 < 0$ will be discussed at the end of this section; in this latter case, the point D is always within the wedge as $t\to\infty$.

From (14*a*), we see that $\Psi(x,y,T)$ depends explicitly on T, as well as implicitly through the variable $\mathscr{G} = (x/T - U_2)/\Delta U$. This suggests the introduction of a new variable of integration, say $\xi = (x/T - U_2)/\Delta U$. After substituting (14*a*) into (15*b*), we arrive at one of our central results,

$$v(x,1,t) = \frac{x^{\frac{1}{2}}\,\mathrm{e}^{\mathrm{i}\omega_* t}}{2\Delta U}\int_0^1 \left\{\exp\left[x\frac{h_0(\xi)-\mathrm{i}\omega_*/\Delta U}{\xi+U_2/\Delta U}\right] \times \frac{\mathscr{F}_1[k_0(\xi)]}{[-h_0^+(\xi)\,(\xi+U_2/\Delta U)^3]^{\frac{1}{2}}} + \mathrm{CC}(\omega_*)\right\}\mathrm{d}\xi + \text{c.c.}, \tag{16}$$

where $\mathrm{CC}(\omega_*)$ denotes the complex conjugate of the term immediately preceding it, provided that we first replace ω_* by $(-\omega_*)$. Equation (16) is valid for large positive x. Note that the quantities needed in the evaluation of (16) are defined in (10) and (14); $\Delta U = U_1 - U_2 > 0$.

Roughly speaking, (16) represents the spatial instability mode (at frequency ω_*) as a superposition of wave packets. All the packets that have reached the point x at time t contribute to the integral; the natural variable of integration is ξ, which is

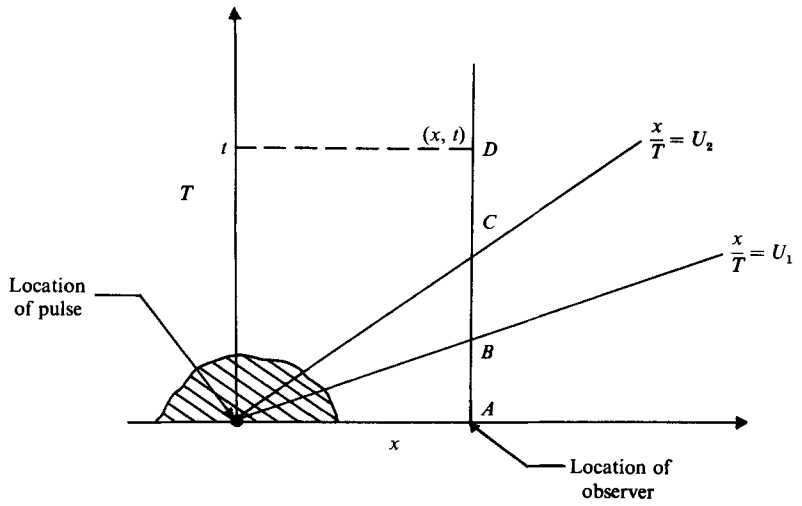

FIGURE 4. Wave diagram of the Green function in propagation space (x, T) for the piecewise linear profile.

essentially the modified observer velocity $\mathscr{G}$. If (16) indeed represents a spatial mode, its large-x dependence must be of the form $\exp(ik_* x)$, where k_* is the wavenumber. Thus, the $x^{\frac{1}{2}}$ factor in the numerator must be cancelled by an identical factor in the denominator. This implies that the integral in (16) should contain a factor $x^{-\frac{1}{2}}$ for large x; therefore, the use of the saddle-point method for the evaluation of the integral is strongly suggested. This evaluation is done by analytically continuing the integrand of (16) into the complex ξ-plane and then by deforming the contour of integration through the saddle point. This can always be done rigorously.

These contour deformations may be described very conveniently in terms of figure 3(*b*). From the origin ($\xi = 0$), the contour is deformed along a short segment that moves into the first quadrant. Along this path, the exponential in (16) is purely oscillatory and the main contribution to the integral comes from $\xi = 0$; this contribution is not greater than $O(1/x)$ since the path is at 'sea level'. At a certain point along this path, we switch to the contour that takes the integration to the right and up through the saddle point and then down to 'sea level' again. Along this latter contour, the imaginary part of the argument of the exponential in (16) is constant and the principal contribution to the integral comes from the saddle point. Finally, it is possible to integrate from the saddle-point path to $\xi = 1$ along 'sea level'. The contribution from this third portion of the contour is once again no greater than $O(1/x)$. No singularities are crossed during this contour deformation. The fact that it is possible to start and end the integration at 'sea level' comes from the observation that $\mathscr{G} = \xi = 1$ and $\mathscr{G} = \xi = 0$ correspond to the leading and trailing edges of the wave packet. At these points, the total growth rate vanishes.

The formal calculation of the saddle point is quite straightforward once it is realized (see (14*b*), (12*b*)) that

$$\frac{\mathrm{d}h_0(\xi)}{\mathrm{d}\xi} = \mathrm{i}k_0(\xi). \tag{17a}$$

The saddle point ξ_* satisfies

$$\mathrm{i}\omega_* = \omega_1[k_0(\xi_*)], \tag{17b}$$

where $k_0(\xi_*)$ is the analytic continuation of $k_0(\mathscr{G})$ (see (13)). We recognize (17*b*) as a statement of spatial instability: At the saddle point ξ_*, the complex wavenumber

$k_* = k_0(\xi_*)$ is such that the real part of the unstable dispersion relation, $\omega_1(k_*)$, vanishes and the imaginary part is equal to the forcing frequency ω_*.

The actual evaluation of the integral in (16) reconfirms our observation on spatial instability. We find (Duff & Naylor 1966, p. 318)

$$v(x,1,t) \sim -\mathrm{i}(\pi/2)^{\frac{1}{2}}\, \mathrm{e}^{\mathrm{i}\omega_* t} \frac{\mathscr{F}_1(k_*)\, \mathrm{e}^{\mathrm{i}k_* x}}{(\partial\omega_1/\partial k)_*} + \text{c.c.}, \tag{18a}$$

where, to repeat, k_* is defined by

$$\omega_1(k_*) = \mathrm{i}\omega_* \text{ (given)} \tag{18b}$$

and the unstable dispersion relation $\omega_1(k)$, and $\mathscr{F}_1(k)$ are given by (10a, b). Clearly, (18a) is a spatial instability mode. Note that for k_* to lie in the right-hand half of the complex wavenumber plane, ω_* must be negative – this is clear from (10a).

Our results for the spatial instability mode are valid as long as the two external streams are moving in the same direction. On the other hand, when the streams are counter-flowing, say $U_1 > 0$ and $U_2 < 0$, a spatial instability mode cannot arise from the initial-value problem. In order to see this, substitute (14a) into (15b) to obtain

$$v(x,1,t) = \frac{\mathrm{e}^{\mathrm{i}\omega_* t}}{2\Delta U} \int_0^\tau \left[\exp\left\{ T\left[h_0(\eta) - \frac{\mathrm{i}\omega_*}{\Delta U} \right] \right\} \frac{\mathscr{F}_1[k_0(\eta)]}{[-T h_0^+(\eta)]^{\frac{1}{2}}} + \mathrm{CC}(\omega_*) \right] \mathrm{d}T + \text{c.c.}, \tag{19a}$$

where

$$\eta = \frac{x}{T} - \frac{U_2}{\Delta U}. \tag{19b}$$

For large values of $\tau = \Delta U t$, the dominant contribution to integral (19a) comes from the upper limit, since now the point D (see figure 4) is always within the wedge formed by the two rays $x/T = U_1, U_2$. Furthermore, the variable η is slowly changing at the upper limit, so that (19a) can be approximated as

$$v(x,1,t) \sim \frac{\mathrm{e}^{\mathrm{i}\omega_* t}}{2\Delta U} \left[\frac{\mathscr{F}_1[k_0(\eta_\infty)]}{[-h_0^+(\eta_\infty)]^{\frac{1}{2}}} \int^\tau \exp\left\{ T\left[h_0(\eta_\infty) - \frac{\mathrm{i}\omega_*}{\Delta U} \right] \right\} \frac{\mathrm{d}T}{T^{\frac{1}{2}}} + \mathrm{CC}(\omega_*) \right] + \text{c.c.} \tag{20a}$$

where

$$\eta_\infty = -\frac{U_2}{\Delta U} > 0. \tag{20b}$$

Clearly (20a) is not a spatial instability mode since, among other things, it is independent of x. When the streams are counterflowing, it is possible to take the limit of (x/t) as $t \to \infty$, x fixed (this limit is, of course, zero) and still remain within the wedge containing the exponentially large part of the Green function. Therefore, all the perturbation quantities will grow in time without bound at a fixed x. In this case, the base flow is said to be absolutely unstable. We shall have more to say about this and a related concept (convective instability) in the next section.

6. Discussion and conclusions

The principal results of this paper are (14a) and (18a): These equations describe not only the general structure of wave packets and spatial instability modes – this much is already known from the work of Gaster (1968, 1975), Huerre & Monkewitz (1985), and others – but also establish the explicit connection between the perturbations in the flow and the external disturbances that generate them. This connection, which can be derived only by solving the initial-value problem, contains

what might be termed (at least loosely) the 'receptivity' of the flow. We are not aware of any other work that explicitly examines the receptivity of free shear flows, although the paper by Huerre & Monkewitz certainly contains this information implicitly.

With reference to our expression for the wave packet (14*a*), the receptivity of the flow is contained in $\mathscr{F}_1(k)$. Although the specific expression for this quantity, as given by (10*b*), is valid for the piecewise linear profile only, the arguments that lead to the spatial instability mode are perfectly general. In other words, if $\mathscr{F}_1(k)$ is a measure of the receptivity of the flow in terms of wave packets, then this same quantity divided by the (complex) group velocity (which is $\partial\omega_1(k)/\partial k$) is a measure of the receptivity of the flow in terms of spatial instability modes (18*a*). This is a powerful new result. Of course, for the spatial instability mode, the amplitude or receptivity is evaluated at the spatial wavenumber (as a function of the excitation frequency) whereas for the packet, it is evaluated at the saddle point (as a function of the observer velocity). Therefore, the two receptivities are not proportional to each other in numerical value; they are merely proportional to each other in functional form. This, we think, is a useful and general result. We next discuss some of the characteristics of wave packets and instability modes.

6.1. *Wave packets*

We begin our discussion of wave packets with some well-known facts. Apart from the complex amplitude $\mathscr{F}_1(k)$, the other factors in (14*a*) are determined completely in terms of the dispersion relation. Essentially, the packet grows exponentially in time (actually with τ), with growth rate $\mathrm{Re}\,[h_0(\mathscr{G})]$, provided that $\mathscr{G}$ is in the range $(0, 1)$. The Doppler-shifted frequency is $\mathrm{Im}\,[h_0(\mathscr{G})]$. These results are shown in figure 5. The maximum growth rate at $\mathscr{G} = 0.5$ equals the maximum growth rate of temporal stability theory, and the saddle point is on the real axis at $k = k_0 \approx 0.4$ (see figures 2 and 3).

The two points $\mathscr{G} = 0, 1$ define the two bounding rays of figure 4. These two rays contain the exponentially large part of the packet at each instant in time. The growth rate of the packet reaches a maximum for an observer moving at the shear-layer average speed, U_m, and it is symmetric for observers moving faster or slower than this speed. The frequency is approximately linear with $\mathscr{G}$ – this implies that $\mathrm{Re}[k_0(\mathscr{G})]$ is relatively insensitive to variations in $\mathscr{G}$ except at the leading and trailing edges of the packet. In other words, the real part of the wavenumber (i.e. the 'physical' wavenumber) is more or less the same throughout the entire packet. The centre of the packet is convecting at speed U_m.

It is interesting to compare the growth rates and frequencies of wave packets in the piecewise linear and tanh base flows. Figure 5 shows that the difference is largely negligible, with one exception. This exception has an important bearing on the absolute and convective instabilities of these flows. The upper ray in figure 4 will be vertical when $U_2 = 0$ (piecewise linear) or $U_2 \approx -0.143U_1$ (tanh); with the slightest amount of reverse flow, the piecewise linear profile is absolutely unstable, whereas the tanh profile can tolerate a small amount of it before becoming absolutely unstable. Therefore, it seems quite reasonable to postulate that coflowing shear layers are convectively unstable and spatial instability modes aways arise in them because of periodic excitation.

In figure 6, we examine the wave-like shape and amplitude of the packet at a typical instant of time (say, $\tau = 50$). We plot the transverse velocity component at the upper interface, $v(x, 1, t)$, as a function of the dipole location y_0. It is interesting

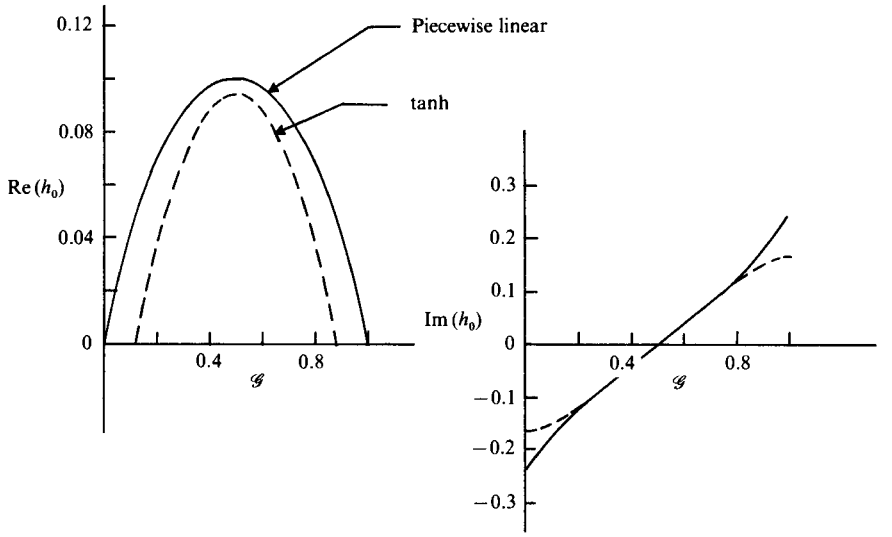

FIGURE 5. Growth rate and Doppler-shifted frequency of wave packet as a function of observer velocity, $\mathscr{G} = (x/t - U_2)/\Delta U$.

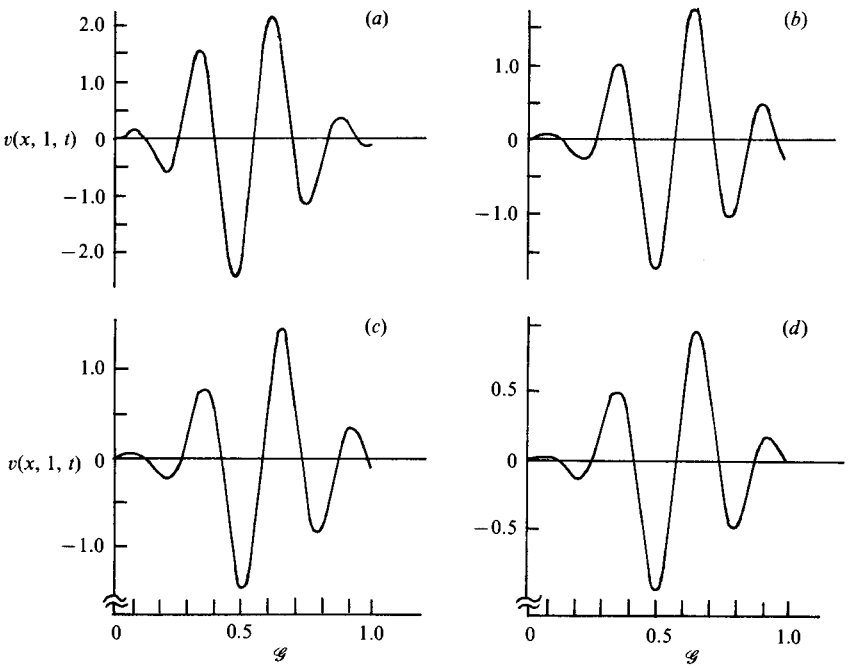

FIGURE 6. Transverse velocity in wave packet at upper edge of shear layer as a function of observer velocity, $\mathscr{G} = (x/t - U_2)/\Delta U$, for parameter values of dipole location: (*a*) $y_0 = 0$; (*b*) 0.6; (*c*) 0.9; (*d*) 2.0 ($\tau = 50$).

to note that as the dipole is brought closer to the upper interface, the peak velocity there actually decreases (refer to the graphs for $y_0 = 0, 0.6, 0.9$). On the other hand, a vortex dipole deposited well outside the shear layer ($y_0 = 2$) can still produce a wave packet of substantial amplitude. In summary, although a shear layer is most sensitive or receptive to disturbances on its centreline, perturbation well outside the layer can still produce large fluctuations within the layer.

At larger values of time, the general wave-like character of the packet is unaltered, although its amplitude is greater because of the exponential growth associated with the instability of the base flow. The streamwise extent of the packet is proportional to time t, and this might suggest that the packet is dispersive in the classical sense. This conclusion is wrong, and perhaps the best counterexample is the one we are studying in this paper. Here, as already pointed out in §4, the phase speed is $\frac{1}{2}(U_1+U_2) = \text{const}$. Therefore, the unstable modes are non-dispersive – the streamwise spreading of the packet arises from variations in growth rate rather than from variations in phase velocity with wavenumber. Finally, note that the fractional change per wavelength in the amplitude is by no means small, so that the square of the amplitude cannot be interpreted as a measure of the local kinetic energy of the wave packet.

6.2. *Spatial instability modes*

The general structure of a two-dimensional spatial instability mode is well known and is extremely simple [i.e. $\exp(\mathrm{i}\omega_* t)\exp(\mathrm{i}k_* x)$], where the complex wavenumber k_*, and the excitation frequency ω_*, are connected by dispersion relation (18*b*). Mathematically, one thinks of a spatial instability mode as the residue arising from the pole at ω_* in the complex frequency domain (say, through the use of a Laplace transform in time). In the present paper we have taken a totally different approach. This approach shows how spatial modes can be interpreted as a superposition of wave packets.

Very roughly speaking, a continuously oscillating source emits a wave packet at each instant of time. At the current time, the location and amplitude of each packet depends on its emission time – those packets that were 'born' at the earliest times are the farthest downstream and have the largest amplitudes. For this reason, there will be a spatial variation in the amplitude (with x) which, in fact, leads to a spatial instability mode. The primary contribution in the superposition integral comes from a saddle point rather than a pole (see (17*b*)). We believe the present method is extremely powerful in the study of three-dimensional instability waves generated by harmonically oscillating and spatially compact disturbances in the flow.

At this point, we have to be a bit more precise as to what we mean by the receptivity of the flow. Since no general definition exists and our objectives are quite modest and specific, we define the receptivity $\mathscr{R}$, where

$$\mathscr{R} = \left| \frac{\Delta U \mathscr{F}_1(k_*)}{(\partial\omega_1/\partial k)_*} \right|. \tag{21}$$

We recognize $\mathscr{R}$ as the amplitude of our spatial instability mode (18*a*) subject to the (arbitrary) normalization condition that the Rayleigh mode for the v-velocity assumes the value $(-\mathrm{i}(\pi/2)^{\frac{1}{2}}/\Delta U)$ on $y = 1$. The factor ΔU in (21) ensures that the receptivity depends only on the 'similarity' parameters $\omega_*/\Delta U$, $U_\mathrm{m}/\Delta U$ (essentially the inverse of the velocity ratio) and the source location y_0. This definition is quite adequate because it tells us how the transverse component of the velocity, $v(x, y, t)$, varies (at fixed x, y and t) as the dipole is moved about or its frequency is changed.

A typical result is shown in figure 7. A most striking feature of this figure is the very large increase (roughly exponential) in the receptivity $\mathscr{R}$ with increasing frequency, at a fixed value of the dipole coordinate, say $y_0 = 0$. For example, $v(x, 1, t)$ would be about ten times larger at $-\omega_*/\Delta U = 0.45$ than at 0.1 in the initial regions of the flow, where any differences in the growth rates may be ignored (i.e. where x

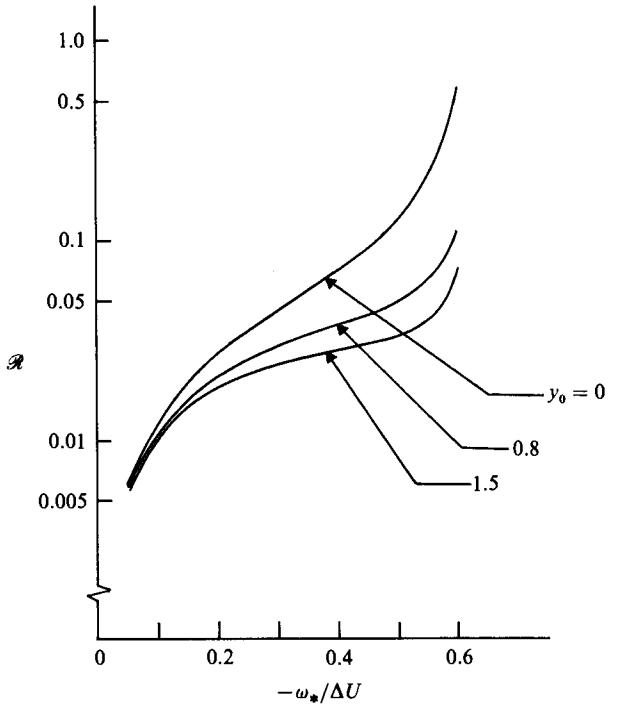

FIGURE 7. Receptivity of shear layer as a function of frequency for parametric values of source location, $U_m/\Delta U = 1$ ($\Delta U = 1$).

is 'small'). Perhaps more correctly, our shear layer is ten times more receptive to this higher-frequency excitation than to the lower one. We believe that these remarks are quite general, and qualitatively apply to other shear layers, although the very rapid increase in the receptivity near the neutral point (i.e. at $-\omega_*/\Delta U \approx 0.6$) is possibly peculiar to our profile.

An explanation for these results is as follows. Without too much difficulty, the Rayleigh equation can be made self-adjoint so that the Green function will become symmetric in the field and source coordinates, y and y_0, respectively. On the other hand, very crudely speaking, an instability mode behaves as $\exp(-ky)$, $y > 0$, or $\exp(\omega_* y)$ since, roughly, $-\omega_* \sim k$. Now all the modes are arbitrarily normalized so that they assume identical values at $y = 1$ (see just below (21)). This implies that at $y = 0$ the modes behave as $\exp(k)$ and, upon interchanging y with y_0, we find that the receptivity, as defined above, varies as $\exp(k)$ or as $\exp(-\omega_*)$. In a nutshell, the exponential increase in the receptivity with frequency at (say) $y = 1$, due to a source at $y_0 = 0$, is caused by the exponential decrease in the mode between the two points $y = 0$, 1.

At a given frequency (say, $-\omega_*/\Delta U = 0.3$), the receptivity of the shear layer decreases as the dipole is moved away from the centreline. This behaviour is consistent with our findings for a wave packet, and it is also an immediate consequence of the explanation given in the preceding paragraph. Note that, generally, this decrease in receptivity is accepted on physical grounds, based on the argument that a flow is the most sensitive to perturbations that occur near the region at which the phase speed and fluid speed are equal. Furthermore, a given change in the source location is more significant at higher frequencies (the important parameter

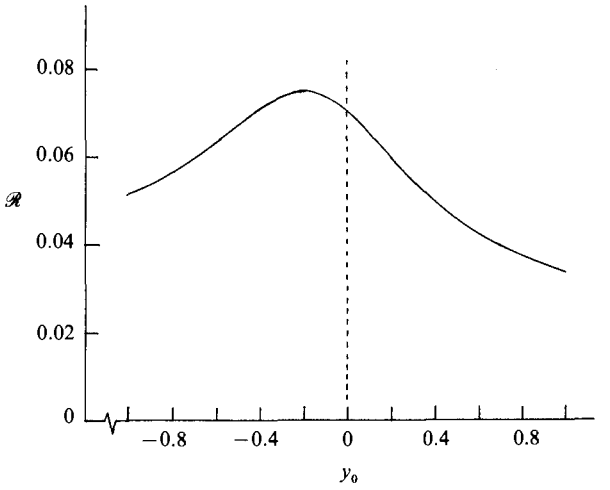

FIGURE 8. Receptivity as a function of dipole location ($\omega_* = -0.4$, $U_1 = 1.5$, $U_2 = 0.5$).

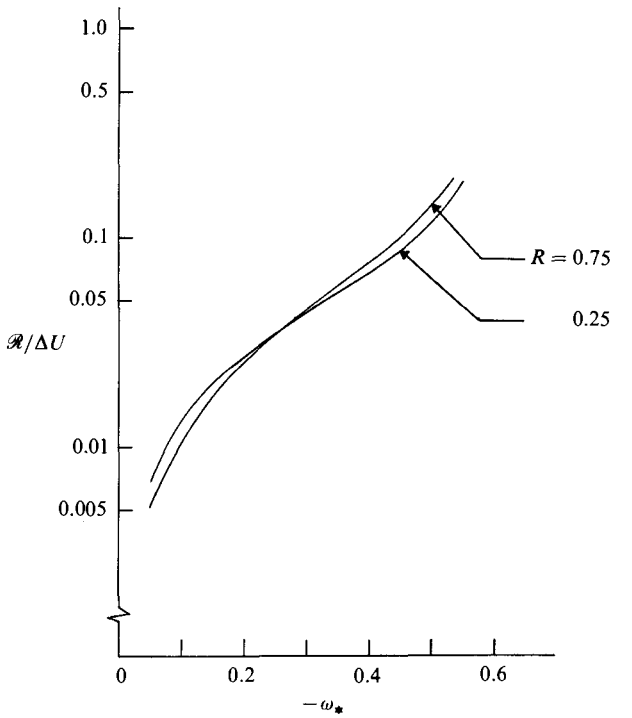

FIGURE 9. Normalized receptivity as a function of frequency for parametric values of velocity ratio $R = \Delta U/2U_m (U_m = 1, y_0 = 0)$.

is the change in y_0 per wavelength) so that one expects any two curves for two different values of y_0 to diverge with frequency. This is indeed what happens in figure 7.

In order to gain a deeper understanding of how the position of the dipole affects the transverse component of the velocity at the upper edge ($y = 1$), we show the receptivity of our shear layer as a function of source location for (approximately) the most unstable frequency (figure 8). It is interesting to note that the curve is not

exactly symmetric about $y_0 = 0$. The bias in the receptivity toward the low-speed side of the layer is caused by a similar bias of the spatial instability mode itself (Michalke 1965). All other things being equal, perturbations at the low-speed side result in larger disturbances in the flow than do perturbations at the high-speed side.

Finally, in figure 9, we show the dependence of the normalized receptivity $\mathscr{R}/\Delta U$ on the velocity ratio, $R = \Delta U/2U_m$, for a dipole located on the centreline. These results, together with the uppermost curve in figure 7, show that the receptivity $\mathscr{R}$ is roughly proportional to the velocity ratio at fixed values of the shear-layer average velocity U_m. In other words, at a given frequency, ω_*, and U_m, the receptivity varies directly as ΔU.

The author is grateful to Professor P. Huerre for an advance copy of the paper by Huerre and Monkewitz. Much of the present work was motivated by a seminar given by Dr. Huerre at the University of Arizona. The financial support of the NASA Lewis Research Center is also acknowledged.

Appendix A

We sketch here the solution of our governing equations (6*a*, *b*) for the given initial and boundary conditions. As remarked in the main section of this paper, the vorticity equation for the piecewise linear base flow can be integrated once and for all. In terms of the Fourier transform of the transverse perturbation velocity $\hat{v}$, we must solve the equation

$$\left(\frac{\partial^2}{\partial y^2} - k^2\right)\hat{v} = \chi(k,t)\,\delta(y-y_0), \tag{A 1}$$

where k is the axial wavenumber, y_0 is the transverse location of the dipole (figure 1), $U_0 = U(y_0)$ and

$$\chi(k,t) = \frac{k^2}{(2\pi)^{\frac{1}{2}}}\exp(-\mathrm{i}kU_0 t) \tag{A 2}$$

and we have assumed that $t > 0$.

The reader should observe that the notation in this Appendix is self-contained and may depart slightly from that in the main body of this paper. Whenever this occurs, we point out explicitly this difference.

The principal task ahead of us is to solve (A 1) with decaying boundary conditions as $|y| \to \infty$ and suitable matching conditions across the interfaces at $y = \pm 1$. Let us first concentrate on the case when the dipole is located within the shear layer, $|y_0| \leqslant 1$.

For this case there are four regions of interest, and in each of these, the solution for $\hat{v}$ can be written as a linear combination of $\exp(\pm\kappa y)$, where κ is the correctly chosen square root, $(k^2)^{\frac{1}{2}}$ as given by (8). By elementary considerations we have

$$\hat{v} = \begin{cases} A\,\mathrm{e}^{-\kappa(y-1)} & (y \geqslant 1), \\ A\cosh[\kappa(y-1)] + C\sinh[\kappa(y-1)] & (y_0 < y \leqslant 1), \\ B\cosh[\kappa(y+1)] + E\sinh[\kappa(y+1)] & (-1 \leqslant y < y_0), \\ B\,\mathrm{e}^{+\kappa(y+1)} & (y \leqslant -1), \end{cases} \tag{A 3}$$

where (A 3) already satisfies the decaying boundary conditions at $|y| \to \infty$ and the continuity of $\hat{v}$ across the interfaces. Note that A, B, C and E are coefficients depending on time (but not on y).

We shall use $A = A(t)$ and $B = B(t)$ as our principal variables since $C(t)$ and $E(t)$ can be readily expressed in terms of the former. This is accomplished by enforcing the usual matching conditions across the source location $y = y_0$. The final result is

$$\left.\begin{matrix} C \\ E \end{matrix}\right\} \sinh 2\kappa = \left.\begin{matrix} A \\ -B \end{matrix}\right\} \cosh 2\kappa \left.\begin{matrix} -B \\ +A \end{matrix}\right\} + \frac{\chi(k,t)}{\kappa} \sinh[\kappa(y_0 \pm 1)]. \tag{A 4}$$

The equations for $A(t)$ and $B(t)$ come from the requirement that the Fourier transform of the pressure is continuous across the interfaces. This requirement can be readily satisfied by using the linearized x-component of the momentum equations. After some straightforward algebra we arrive at

$$e^{2\kappa}\frac{d}{dt}\begin{Bmatrix} \tilde{A} \\ \tilde{B} \end{Bmatrix} - \frac{d}{dt}\begin{Bmatrix} \tilde{B} \\ \tilde{A} \end{Bmatrix} = \pm\tfrac{1}{2}ik\Delta U \begin{Bmatrix} \tilde{B} \\ \tilde{A} \end{Bmatrix} \mp \tfrac{1}{2}ik\Delta U\left(e^{2\kappa} - \frac{\sinh 2\kappa}{\kappa}\right)\begin{Bmatrix} \tilde{A} \\ \tilde{B} \end{Bmatrix}$$

$$\pm ik\tilde{\chi}(k,t)\frac{\sinh[\kappa(y_0 \pm 1)]}{\kappa}\left(U_0 - \begin{Bmatrix} U_1 \\ U_2 \end{Bmatrix}\right), \tag{A 5}$$

where $(\tilde{\cdot}) = (\cdot)\exp(+ikU_m t)$, $U_m = \frac{1}{2}(U_1 + U_2)$ and $\Delta U = U_1 - U_2$. Note, in particular, that $(\tilde{\cdot})$ does not denote complex conjugation. The time derivatives in (A 5) come from the fact that the x-component of the momentum equation contains the term $\partial u/\partial t$. The choice of the tilde variables makes (A 5) entirely symmetric and it is essentially equivalent to a Galilean transformation in which the observer is moving at the average shear-layer velocity U_m.

If we diagonalize the left-hand side of (A 5), we simplify the equations for $\tilde{A}$ and $\tilde{B}$. We also give these equations for reference:

$$\frac{1}{\Delta U ik/\kappa}\frac{d}{dt}\begin{Bmatrix} \tilde{A} \\ \tilde{B} \end{Bmatrix} = \begin{bmatrix} a_{11} & a_{12} \\ a_{21} & a_{22} \end{bmatrix}\begin{bmatrix} \tilde{A} \\ \tilde{B} \end{bmatrix} + \begin{Bmatrix} S_1 \\ S_2 \end{Bmatrix}, \tag{A 6a}$$

where

$$a_{11} = a_{11}(k) = \tfrac{1}{4} - \Gamma\cosh 2\kappa, \tag{A 6b}$$

$$a_{12} = a_{12}(k) = \Gamma - \tfrac{1}{4}e^{-2\kappa}, \tag{A 6c}$$

and $\Gamma = \Gamma(k) = \kappa/(2\sinh 2\kappa)$. Furthermore,

$$a_{21} = a_{21}(k) = -a_{12}(k), \tag{A 6d}$$

$$a_{22} = a_{22}(k) = -a_{11}(k). \tag{A 6e}$$

The two inhomogeneous terms S_1 and S_2 are given by

$$S_1 = \frac{\tilde{\chi}(k,t)}{2\Delta U\sinh 2\kappa}\{(U_0 - U_1)\sinh[\kappa(y_0+1)] - (U_0 - U_2)e^{-2\kappa}\sinh[\kappa(y_0-1)]\}, \tag{A 6f}$$

$$S_2 = \frac{\tilde{\chi}(k,t)}{2\Delta U\sinh 2\kappa}\{(U_0 - U_1)e^{-2\kappa}\sinh[\kappa(y_0+1)] - (U_0 - U_2)\sinh[\kappa(y_0-1)]\}. \tag{A 6g}$$

The final step is to solve (A 6a) explicitly with the given initial conditions. Rather than enforcing the null initial conditions at $t = 0^-$, it is far more convenient to transfer these conditions to $t = 0^+$ by integrating (1a, b) across $t = 0$. In other words, the instant after the dipole has been switched on, we find

$$\left.\begin{matrix} A(0^+) = \tilde{A}(0^+) \\ B(0^+) = \tilde{B}(0^+) \end{matrix}\right\} = -\frac{\chi(k,0)}{2\kappa}e^{-\kappa}e^{\pm\kappa y_0}. \tag{A 7}$$

In order to write down the solution of (A 6a) with initial conditions (A 7), we need some preliminary definitions. Let

$$\lambda(k) = \tfrac{1}{4}\{[\mathrm{e}^{-4\kappa} - (1-2\kappa)^2]^{\frac{1}{2}}\}, \tag{A 8a}$$

$$\mathscr{D}(k) = (\tfrac{1}{2}\kappa y_0)^2 + \lambda^2(k), \tag{A 8b}$$

and

$$\left.\begin{matrix} a(k) \\ b(k) \end{matrix}\right\} = \tfrac{1}{4}\chi(k,0)\,(y_0 \mp 1) \times \frac{\sinh[\kappa(y_0 \pm 1)]\,[\frac{1}{2}\mathrm{e}^{-2\kappa} \mp (y_0 \pm 1)\,\Gamma(k)] \pm (y_0 \pm 1)\,\Gamma(k)\,\mathrm{e}^{-2\kappa}\sinh[\kappa(y_0 \mp 1)]}{\mathscr{D}(k)}. \tag{A 8c}$$

Finally, the solutions for $\tilde{A}(t)$ and $\tilde{B}(t)$ become

$$\tilde{A}(t) = \frac{\mathrm{e}^{\lambda\tau}\{[A(0^+)-a]\,(\lambda + \mathrm{i}a_{11}) + \mathrm{i}a_{12}[B(0^+)-b]\}}{2\lambda} + \frac{\mathrm{e}^{-\lambda\tau}\{-\mathrm{i}a_{12}[B(0^+)-b] + [A(0^+)-a]\,(\lambda - \mathrm{i}a_{11})\}}{2\lambda} + a\exp[-\mathrm{i}k(U_0 - U_\mathrm{m})\,t], \tag{A 9a}$$

$$\tilde{B}(t) = \frac{\mathrm{e}^{\lambda\tau}\left\{[A(0^+)-a]\dfrac{(\lambda-\mathrm{i}a_{11})\,(\lambda+\mathrm{i}a_{11})}{\mathrm{i}a_{12}} + [B(0^+)-b]\,(\lambda - \mathrm{i}a_{11})\right\}}{2\lambda} + \frac{\mathrm{e}^{-\lambda\tau}\left\{-[A(0^+)-a]\dfrac{(\lambda-\mathrm{i}a_{11})\,(\lambda+\mathrm{i}a_{11})}{\mathrm{i}a_{12}} + [B(0^+)-b]\,(\lambda + \mathrm{i}a_{11})\right\}}{2\lambda} + b\exp[-\mathrm{i}k(U_0 - U_\mathrm{m})\,t], \tag{A 9b}$$

where, in (A 9a, b), the quantities a, λ, etc. are evaluated at k [i.e. $a = a(k)$, etc.] and $\tau = \Delta U t k/\kappa$.

We now recognize $A(0^+)$ and $B(0^+)$ as essentially A_0 and B_0 of (10b) and the first two terms of (A 9a) without the factors $\exp(\pm\lambda\tau)$, correspond to $\mathscr{F}_1$ and $\mathscr{F}_2$ of (9).

When the dipole is located outside the shear layer (i.e. $|y_0| > 1$), we have the somewhat simpler result $a = b = 0$. In other words, the inhomogeneous terms S_1 and S_2 on the right-hand side of (A 6a) are identically zero. Furthermore,

$$\left.\begin{matrix} A(0^+) = \tilde{A}(0^+) \\ B(0^+) = \tilde{B}(0^+) \end{matrix}\right\} = -\frac{\chi(k,0)}{2\kappa}\,\mathrm{e}^{-\kappa|y_0|}\exp[\pm\kappa\,\mathrm{sgn}\,(y_0)], \tag{A 10}$$

where $\mathrm{sgn}\,(y_0) = \pm 1$ according to $y_0 > 0$ or $y_0 < 0$. Otherwise, (A 9a, b) hold for $\tilde{A}(t)$ and $\tilde{B}(t)$.

REFERENCES

Balsa, T. 1987 On the spatial instability of piecewise linear free shear layers. *J. Fluid Mech.* **174**, 553–563.

Betchov, R. & Criminale, W. O. 1966 Spatial instability of the inviscid jet and wake. *Phys. Fluids* **9**, 359–362.

Betchov, R. & Criminale, W. O. 1967 *Stability of Parallel Flows*. Academic.

Bleistein, N. & Handelsman, R. 1975 *Asymptotic Expansion of Integrals*. Holt, Rinehart and Winston.

Craik, A. D. D. & Criminale, W. O. 1986 Evolution of wavelike disturbances in shear flows: a class of exact solutions of the Navier–Stokes equations. *Proc. R. Soc. Lond.* A**406**, 13–26.

CRIMINALE, W. O. & KOVASZNAY, L. G. 1962 The growth of localized disturbances in a laminar boundary layer. *J. Fluid Mech.* **12**, 59–80.

DRAZIN, P. G. & REID, W. H. 1981 *Hydrodynamic Stability.* Cambridge University Press.

DUFF, G. F. D. & NAYLOR, D. 1966 *Differential Equations of Applied Mathematics.* Wiley.

FARRELL, B. F. 1982 The initial growth of disturbances in a baroclinic flow. *J. Atmos. Sci.* **38**, 1663–1686.

FARRELL, B. F. 1984 Modal and non-modal baroclinic waves. *J. Atmos. Sci.* **41**, 668–673.

GASTER, M. 1968 The development of three-dimensional wave packets in a boundary layer. *J. Fluid Mech.* **32**, 173–184.

GASTER, M. 1975 A theoretical model of a wave packet in the boundary layer on a flat plate. *Proc. R. Soc. Lond* A **347**, 271–289.

GASTER, M., KIT, E. & WYGNANSKI, I. 1985 Large-scale structures in a forced turbulent mixing layer. *J. Fluid Mech.* **150**, 23–39.

GLEZER, A., WYGNANSKI, I. & BALSA, T. 1986 Spatial and temporal evolution of momentary disturbances in an excited turbulent mixing layer. *Bull. Am. Phys. Soc.* **31**, 1694 (abstract only).

GOLDSTEIN, M. E. 1983 The evolution of Tollmien–Schlichting waves near a leading edge. *J. Fluid Mech.* **127**, 59–81.

GREENSPAN, H. P. & BENNEY, D. 1963 On shear-layer instability, breakdown and transition. *J. Fluid Mech.* **15**, 133–153.

HUERRE, P. & MONKEWITZ, P. 1985 Absolute and convective instabilities in free shear layers. *J. Fluid Mech.* **159**, 151–168.

MATTINGLY, G. E. & CRIMINALE, W. O. 1972 The stability of an incompressible two-dimensional wake. *J. Fluid Mech.* **51**, 233–272.

MICHALKE, A. 1964 On the inviscid instability of the hyperbolic-tangent velocity profile. *J. Fluid Mech.* **19**, 543–556.

MICHALKE, A. 1965 On spatially growing disturbances in an inviscid shear layer. *J. Fluid Mech.* **23**, 521–544.

TATSUMI, T., GOTOH, K. & AYUKAWA, K. 1964 The stability of a free boundary layer at large Reynolds numbers. *J. Phys. Soc. Japan* **19**, 1966–1980.